Title

Sensitivity of Simulated Surface Fluxes to Changes in Land Surface Parameterizations-A Study Using ABRACOS Data

Journal

Journal of Applied Meteorology, 35(3)

ISSN

0894-8763

Authors

Xue, Yongkang
Bastable, Heidi G
Dirmeyer, Paul A
et al.

Publication Date

1996-03-01

DOI

10.1175/1520-0450(1996)035<0386:sossft>2.0.co;2

Peer reviewed

Sensitivity of Simulated Surface Fluxes to Changes in Land Surface Parameterizations—A Study Using ABRACOS Data

YONGKANG XUE

Center for Ocean–Land–Atmosphere Studies, Calverton, Maryland

HEIDI G. BASTABLE

Institute of Hydrology, Wallingford, United Kingdom

PAUL A. DIRMEYER

Center for Ocean–Land–Atmosphere Studies, Calverton, Maryland

PIERS J. SELLERS

GSFC/NASA, Greenbelt, Maryland

(Manuscript received 12 April 1995, in final form 5 September 1995)

ABSTRACT

The simplified Simple Biosphere model (SSiB) has been validated using observed meteorological, turbulent flux, and vegetation property data from the Anglo–Brazilian Amazonian Climate Observation Study (ABRACOS) over a forest clearing site. The results show that SSiB is able to simulate the observed fluxes realistically. The differences between the simulated and observed latent and sensible heat fluxes are less than 10 W m^{-2}. Compared to previous deforestation experiments, the new vegetation dataset produces significantly different latent heat fluxes and surface temperatures in off-line and general circulation model (GCM) simulations. Using the new dataset, the GCM simulated surface temperature is about 2 K higher, and the simulated latent heat flux is about 25 W m^{-2} lower than that generated using a previous dataset. These differences can be expected to result in substantially different responses in rainfall and atmosphere circulation. The parameters that are most significant in producing such large differences are leaf area index and soil properties. This study again demonstrates that to realistically assess the climatic impact of land surface degradation a realistic specification of the land surface conditions within GCMs is crucial.

1. Introduction

For some years now, general circulation models (GCMs) have been used to predict the effects of large-scale deforestation on climate (e.g., Henderson-Sellers and Gornitz 1984; Dickinson and Henderson-Sellers 1988; Lean and Warrilow 1989; Shukla et al. 1990; Nobre et al. 1991; Dirmeyer 1992; Henderson-Sellers et al. 1993; Polcher and Laval 1994; Dirmeyer and Shukla 1994; and Sud et al. 1995). Although all these studies simulated a higher surface temperature and lower evaporation rate in the deforested areas, they disagree on the degree of change in the surface temperature and evapotranspiration rates and the impact of deforestation on precipitation. Most models predict a reduction in mean rainfall in the deforestation scenario, whereas others predict no net change, or even higher precipitation. Besides the differences in model structure and formulation, these differences in predictions could be partly due to erroneous specification of the land surface characteristics of forest and deforested areas.

The validity of model predictions is highly dependant upon having representative parameters and real data from both forested and cleared areas for model calibration and validation, respectively. It would be impossible to make valid climate predictions without such information. Conditions above primary Amazonian rainforest have been described by Shuttleworth et al. (1985) and Shuttleworth (1988), and these measurements have been used in the calibration of land surface models within GCMs (e.g., Lloyd et al. 1988, Sellers et al. 1989).

Currently, the Anglo–Brazilian Amazonian Climate Observation Study (ABRACOS) is the only comprehensive observational study of land surface–atmosphere interactions in large-scale clearings caused by

Corresponding author address: Dr. Yongkang Xue, Center for Ocean-Land-Atmosphere Studies, 4041 Powder Mill Road, Suite 302, Calverton, MD 20705.
E-mail: xue@cola.iges.org

tropical deforestation (Shuttleworth et al. 1991). The main objective of ABRACOS was to provide comparative data from adjacent forested and cleared areas, and to provide representative parameters and data from clearings for GCM studies. In this study, the observational data from ABRACOS are used to validate the simplified version of the Simple Biosphere model (SSiB) (Sellers et al. 1986; Xue et al. 1991). Several off-line and GCM numerical experiments have been conducted to test the sensitivity of model simulation to the specification of the surface conditions.

2. ABRACOS field experiment

The data used in this study were collected during the first two experimental seasons of ABRACOS at the Fazenda Dimona ranch site (2°19′S, 60°19′W), 100 km north of Manaus in central Amazonia. Mission 1 was conducted from 4 October to 2 November 1990 and mission 2 was conducted from 29 June to 10 September 1991. Further details of the ranch and experimental site are described by Wright et al. (1992), McWilliam et al. (1993), and Bastable et al. (1993).

Incoming and reflected radiation of wavelength 0.3–3.0 μm were measured using upward and downward facing CM-5 Kipp & Zonen (Delft, the Netherlands) pyranometers. Net all-wave radiation was measured by single dome Q*6 net radiometers (REBS, Seattle, Washington). Soil heat flux was measured along a transect using Thornthwaite (Elmer, New Jersey) model 610 soil heat flow disks installed at 5-mm depth. Manufacturer supplied calibrations were used for all the radiation instruments.

Aspirated platinum resistance thermometers, housed in the Institute of Hydrology (United Kingdom) psychrometer screen, measured ambient air and wet-bulb temperatures. The soil temperature was measured at a depth of 10 cm. The thermometers were calibrated against a standard and are accurate to within ±0.1 K. A Didcot Instrument Company (Abingdon, United Kingdom) 0.2-mm-resolution tipping-bucket rain gauge, and wind speed and direction sensors were used. The data were recorded using solid state loggers (Campbell Scientific Ltd., Shepshed, United Kingdom), which sampled every 10 s.

Three measurement systems were used to estimate fluxes of water vapor and sensible heat. A full description can be found in Wright et al. (1992). A Campbell Scientific Ltd. (United Kingdom) Bowen ratio system measured temperature and humidity gradients between two levels (0.9 and 3.2 m) and recorded summary data at 20-min intervals. A logarithmic wind and scaler profile measurement rig with six levels (from 0.5 to 9.0 m) was constructed on an alloy tower. At each level an aspirated psychrometer with wet and dry-bulb thermistors and a polystyrene cup anemometer (Vector Instruments, United Kingdom) were mounted. The Mk 2 "Hydra" eddy correlation device (Shuttleworth et al. 1984) was used to estimate fluxes of water vapor and sensible heat. This instrument comprises an infrared absorption hygrometer, a fine wire thermocouple, and a sonic anemometer, together with a net all-wave radiometer and fast-response cup anemometer. The Hydra logging system samples at 10 Hz and computes and stores an hourly statistical summary of fluxes. There was excellent agreement between the three measurement systems, their data were combined to form a complete hourly time series record for each experimental period.

3. Simplified SiB model (SSiB)

The SSiB biosphere model (Xue et al. 1991) was used in this validation study. The vegetation–soil layer affects the radiative transfer at the surface, the partitioning of surface energy into sensible heat flux and latent heat flux, and the momentum flux. The model attempts to describe the biophysical controls on these exchanges by modeling the vegetation itself so that the exchange processes are mutually consistent. SSiB has three soil layers, one canopy layer, and eight prognostic variables: soil wetness in the three soil layers; temperature at the canopy, ground, surface, and deep soil layers; water stored on the canopy; and snow stored on the ground.

In the radiative transfer submodel, the optical and geometric properties of the leaves and stems, and the optical properties of the soil affect the surface albedo and the attenuation of photosynthetically active radiation (PAR) down through the canopy. The surface albedo is modeled to have a diurnal variation with a minimum at local noon. Since the variation of the albedo with solar angle is quite regular, a quadratic equation is used to describe the albedo and its diurnal variations. The equation was fitted to the results of two-stream radiative transfer model calculations. For a specific vegetation type the albedo α is also a function of the solar zenith angle θ and snow cover S:

$$\alpha = a\cos\theta + b(\cos\theta)^2 + cS + dS^2 + e. \quad (1)$$

The coefficients of the quadratic equation (a, b, c, d, and e) depend on vegetation type.

The resistance to the transfer of water vapor from the canopy and upper soil layer to the adjacent exterior air includes canopy resistance, and soil surface resistance. The results of Camillo and Gurney (1986) were used to curve-fit a simple relationship between soil surface resistance and wetness of the upper 0.5 cm of the soil. The parameterization of the stomatal resistance in SiB was based on the work of Jarvis (1976). An analytic solution for the bulk stomatal resistance was introduced by Sellers (1985). The three stress terms included in this scheme describe the dependence on the atmospheric temperature, the soil water potential, and the vapor pressure deficit, respectively. The original linear stress term for vapor pressure deficit in the first

SiB model of Sellers et al. (1986) caused the stomata to close too early, which often resulted in excessively high surface temperatures and an even higher vapor deficit. A modification, which was tested against field experiment data (FIFE; see Sellers et al. 1992) is used in this version of the model:

$$F(\Delta e) = (1 + h_c \Delta e)^{-1}, \quad (2)$$

where the Δe is the vapor pressure deficit and h_c is a constant that depends on vegetation type. The dependence of water vapor deficit on this factor in both the new formula and old formula for grassland is depicted in Fig. 1. In the new formula, the stomata do not close completely due to the vapor deficit.

Similarity theory was used to calculate the aerodynamic resistance from the canopy to the reference height. Based upon the equations of Paulson (1970) and Businger et al. (1971) a linear relationship between the Richardson number and aerodynamic resistance was developed. The equation for momentum flux transfer is

$$U_* = U_r(C_u^{-1} + C_{un}^{-1}), \quad (3)$$

where U_* is the friction velocity, U_r is the wind velocity at the reference height, C_{un} is the neutral momentum transfer coefficient, and C_u is the nonneutral coefficient. Louis (1979) developed a parameterization scheme in which the total aerodynamic resistance including both neutral and nonneutral parts is a function of Richardson number and surface roughness. The accuracy of this parameterization strongly depends on the surface roughness length. In a biosphere model, the range of values of surface roughness length can be very large. Parameterizing the total resistance may cause large errors. In SSiB, we only parameterize the nonneutral part; C_{un}, which is dependent on vegetation and soil properties, is given by:

$$C_{un}^{-1} = \frac{1}{k_0} \ln\left(\frac{z_m - d}{z_0}\right), \quad (4)$$

where k_0 is von Kármán's constant, z_m is the reference height, d is the displacement height, and z_0 is the roughness height. For the nonneutral part,

$$C_u^{-1} = \begin{cases} 0.315\ \mathrm{Ri}, & -10 \leq \mathrm{Ri} < 0 \\ 66.85\ \mathrm{Ri}, & 0 \leq \mathrm{Ri} \leq 0.16 \end{cases} \quad (5)$$

and

$$\mathrm{Ri} = \frac{g \Delta z \Delta \theta}{\theta (\Delta u)^2}, \quad (6)$$

where g is the gravitational constant, u is the wind speed, and θ is the potential temperature. We have developed some complex exponential equations to relate the bulk Richardson number to surface resistance. These equations have reproduced the results from similarity theory (Xue et al. 1991). The reason we developed linear equations were not only due to the consideration that these equations were more simple and more computationally efficient in a GCM, but also due to concerns about scaling. Eddy flux in each grid point in a GCM is assumed to be the average of the influence of a large number of subgrid-scale eddies. Sud and Smith (1984) found that the relationship between aerodynamic resistances and ensemble mean Richardson number had a tendency to change from exponential to linear. The linear parameterization described here has produced very good flux simulations in many cases (e.g., Shao et al. 1994). The equations for heat flux transfer are

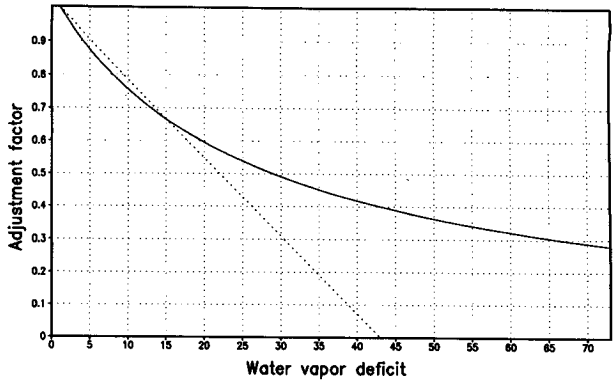

FIG. 1. Dependence of adjustment factor of stomatal resistances on water vapor deficit for grassland. Solid line: new formula; dashed line: old formula.

$$E = \frac{U_*}{(C_{TN}^{-1} + C_{TT}^{-1})}(q_m - q_a) \equiv \frac{(q_m - q_a)}{r_a} \quad (7)$$

for latent heat flux and

$$F = \frac{U_*}{(C_{TN}^{-1} + C_{TT}^{-1})}(T_m - T_a) \equiv \frac{(T_m - T_a)}{r_a} \quad (8)$$

for sensible heat flux. Variables T_m, q_m, T_a, and q_a are the temperatures and specific humidity at the reference height and in the canopy air space, respectively. Parameter C_{TN} is the neutral heat transfer coefficient, r_a is the aerodynamic resistance, and q_a and q_m are the specific humidity in the canopy air space and at the reference height, respectively. Coefficient C_{TN} is given by

$$C_{TN}^{-1} = \frac{1}{k_0}\left(\ln\frac{z_m - d}{z_r - d} + g_3 \ln\frac{z_r - d}{z_2 - d}\right), \quad (9)$$

where z_2 is the height of canopy and g_3 is the ratio of actual r_a to r_a calculated using a log-linear wind profile assumption. It is held constant at 0.75. The depth of transition layer above canopy is z_r. Above this transition layer, the log-linear assumption is valid. Following Sellers et al. (1989), we use

$$Z_r = Z_2 + 11.785 Z_0. \quad (10)$$

TABLE 1. Vegetation parameters.

Vegetation parameters	DATA N	DATA P	Rainforest
Surface albedo	0.18	0.25[a]	
		0.18[b]	0.13
Leaf area index (LAI)	1(M1)[c]	2.2(L1)[d]	
	2(M2)	2.4(L2)	5.0
Greenness	0.7(M1)	0.74(L1)	
	0.9(M2)	0.01(L2)	0.9
Vegetation cover fraction	0.85	0.8(L1)	
		0.8(L2)	0.98
Soil layer thicknesses (m)	0.02, 0.98, 1	0.02, 0.57, 2.9	0.02, 1.47, 2
Soil hydraulic conductivity at saturation (m s^{-1})	2.2E − 5	0.2E − 5	2.0E − 5
Sorption parameter B	6.9	10.4	7.12
Soil water potential at saturation (m)	−0.035	−0.153	−0.08
Porosity	0.59	0.42	0.42
Minimum stomatal resistance (s m^{-1})	140	140	162
Adjustment factor for water vapor deficit	0.020	0.019	0.027
Adjustment factor for temperature	295, 276, 323	308, 276, 327	303, 276, 318
Adjustment factor for soil moisture	1.73, 5.8	1.73, 5.8	1.2, 6.25
Rooting depth (m)	1.0	1.0	1.0
Surface roughness length (m)	0.026	0.076	2.65
Displacement height (m)	0.18	0.26	27.3
Vegetation height (m)	0.28	0.6	35.0

[a] For Nobre experiments.
[b] For Dirmeyer, and Dirmeyer and Shukla experiments.
[c] M1 is the Mission 1 and M2 is the Mission 2.
[d] L1 stands for the first layer and L2 for the second layer.

For the nonneutral heat transfer coefficient, we have

$$C_{TT}^{-1} = f[\mathrm{Ri}(z_m)] + (g_3 - 1)f[\mathrm{Ri}(z_r)] - g_3 f[\mathrm{Ri}(z_2)] \quad (11)$$

for $0 > \mathrm{Ri} > -10$, where

$$f(\mathrm{Ri}) = 0.94\ \mathrm{Ri}. \quad (12)$$

For $0.16 > \mathrm{Ri} > 0$, we have

$$C_{TT}^{-1} = 66.85\ \mathrm{Ri}(z_m) \times \left[1 + \frac{z_r - d}{z_m - d}(g_3 - 1) - g_3 \frac{z_2 - d}{z_m - d}\right]. \quad (13)$$

4. Off-line calibration

In the off-line numerical experiments, we used observed temperature, humidity, and wind at the reference height, precipitation, and net radiation at the surface as forcing to test SSiB. SSiB calculates fluxes and energy components, including the latent heat and sensible heat fluxes, ground heat flux, momentum flux, and upward shortwave and longwave radiation. All these components, with the exception of longwave radiation, were measured during ABRACOS. The model also simulates the water balance at the surface, including the soil moisture content, surface runoff, and drainage. Soil moisture measurements are available, but there were no runoff or drainage measurements made in ABRACOS. The values of vegetation parameters used for off-line validation were from measurements in the ABRACOS field campaign. These vegetation parameter data will be referred to as DATA N in this paper. The values of the major parameters are listed in Table 1. The vegetation data used for previous deforestation experiments (Nobre et al. 1991; Dirmeyer 1992; Dirmeyer and Shukla 1994) are also listed in Table 1; these are referred to as DATA P in this paper.

ABRACOS intensive flux observations were made for a continuous 30-day period during mission 1 (M1) and for 74 days during mission 2 (M2). Since the simulation results for M1 were very similar to M2, and M2 has the longer time series, we show only the comparison between the observed and simulated daily means of latent heat flux, sensible heat flux, ground heat flux, and friction velocity for M2 in Figs. 2a–c. The root-mean-square (rms) errors of the daily mean fluxes for the entire periods of both M1 and M2 are listed in Table 2. Figure 2a shows that the simulated latent heat flux closely follows observations.

TABLE 2. The root-mean-square errors in off-line simulations.

	Latent heat flux (W m^{-2})	Sensible heat flux (W m^{-2})	Ground heat flux (W m^{-2})	Friction velocity (m s^{-1})
Mission 1	9.8	9.7	3.9	0.01
Mission 2	9.4	7.3	4.3	0.01

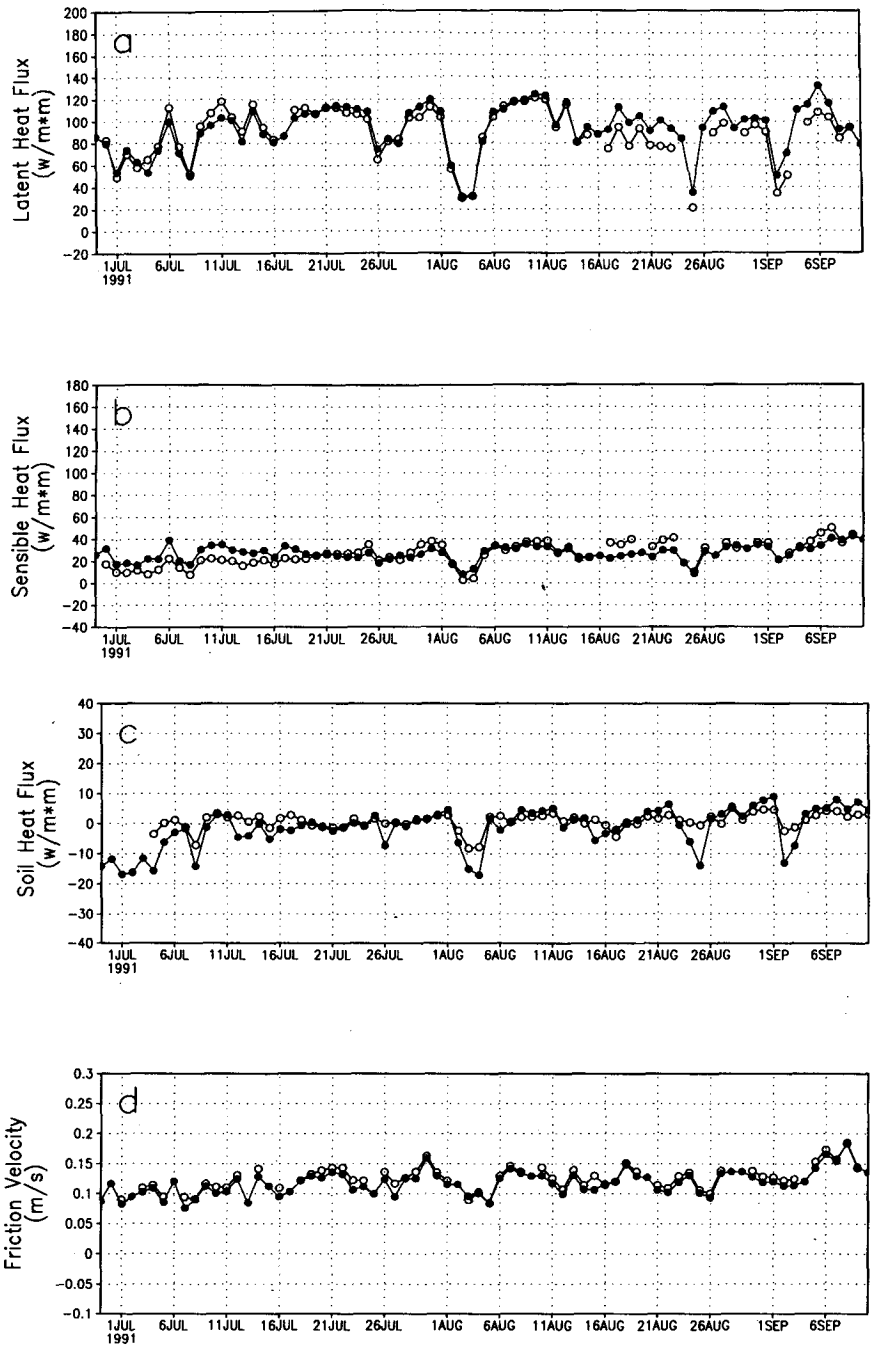

FIG. 2. Daily mean fluxes in mission 2; (a) latent heat flux (W m^{-2}); (b) sensible heat flux (W m^{-2}); (c) ground heat flux (W m^{-2}); (d) friction velocity (m s^{-1}). Open circles: observation; Closed circles: simulation.

The observed latent heat fluxes dropped sharply several times during M2 (3, 4, and 25 August and 2 September). The model simulated such dramatic changes and recovered well. After 16 August, the simulated latent heat fluxes have a systematic positive bias, of about 15 W m^{-2}, which was the major cause of the 9 W m^{-2} rms errors (Table 2) for the entire integration period.

The simulated sensible heat fluxes are also able to follow closely the variations of the observations (Fig. 2b). There is a slight positive bias at the beginning of the first 15-day integration and a minor negative bias

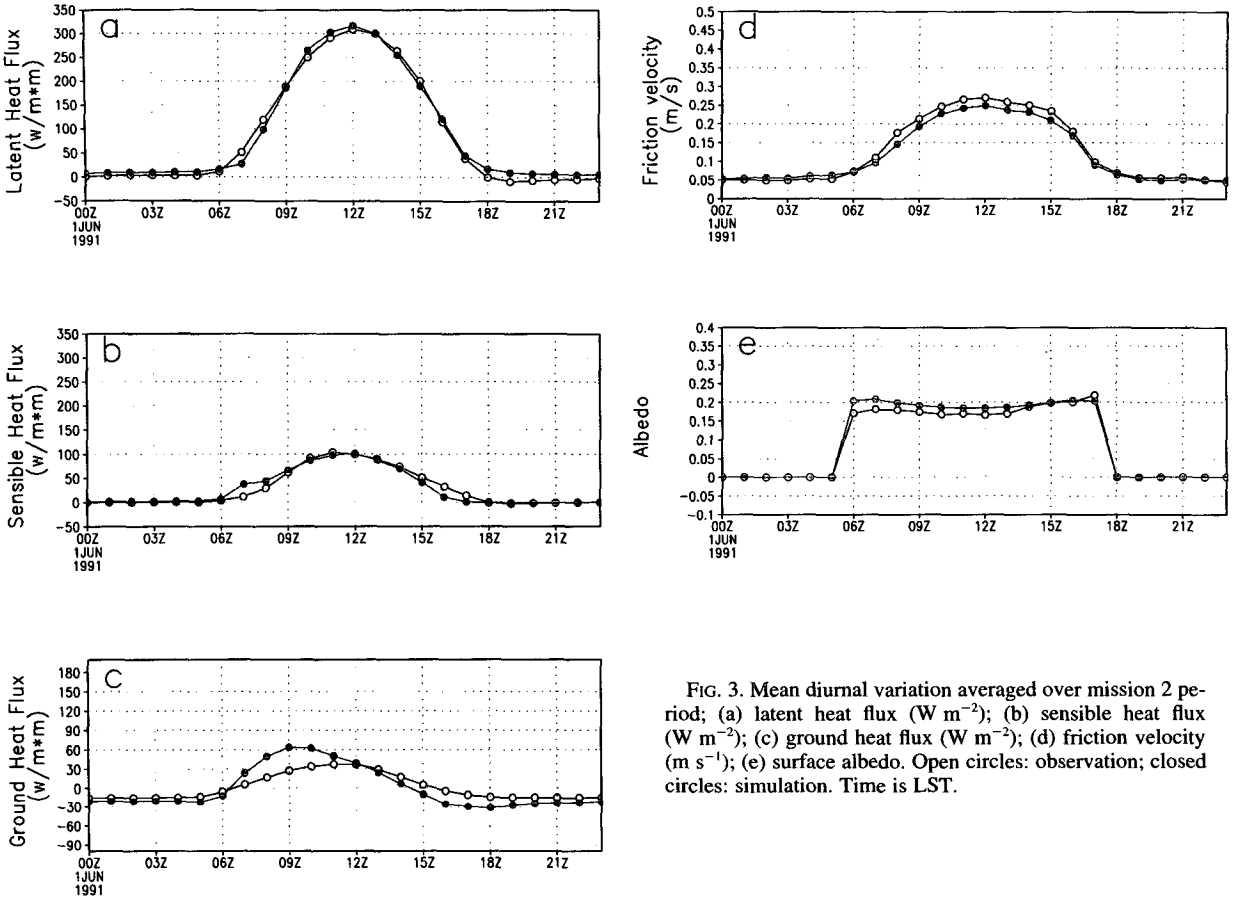

FIG. 3. Mean diurnal variation averaged over mission 2 period; (a) latent heat flux (W m^{-2}); (b) sensible heat flux (W m^{-2}); (c) ground heat flux (W m^{-2}); (d) friction velocity (m s^{-1}); (e) surface albedo. Open circles: observation; closed circles: simulation. Time is LST.

during the later integration period. The total rms error for sensible heat flux was small, about 7 W m^{-2}. The daily mean ground heat fluxes were very small and were well simulated (Fig. 2c). The simulated friction velocity almost precisely followed the observations (Fig. 2d), which supports the morphological parameters used in this dataset. The aerodynamic resistance model was able to correctly simulate the momentum flux transfer. The simulation for M1 (not shown) is very similar to M2, and the rms errors for other flux components are very close to the M2 (see Table 2).

Figures 3a–d and Figs. 4a–d show the diurnal flux variations averaged over the entire period for M2 and M1, respectively. The major differences between the simulated and observed latent heat fluxes are during the night (Figs. 3a and 4a), in particular, at around 1800 local time, when the observed data show either zero or negative evaporation. The model produces positive evaporation during this time. This evaporation is from the soil when the canopy is closed. Most of these differences for M2 occur during the later part of the integration period, as was described earlier.

Although the simulated daily mean ground heat flux is very close to observations, the simulated diurnal variations have a systematic phase shift of about 2–3 h. For a periodic forcing, the peak for surface temperature should be 3 h in advance of the surface heat flux (Dickinson 1983). The force–restore method, which is used in this model to predict surface temperature, assumes the forcing is a periodic function and is largely responsible for the erroneously simulated phase difference.

The simulated friction velocity and sensible heat flux compare well with observation. We note that there is a slight negative bias in the friction velocity simulation around noon. The simulated sensible heat flux in M1 has a larger error at noon. The simulated albedo (Figs. 3e and 4e) is close to the observations. Since the model's albedos are calculated from the soil and vegetation properties, these agreements again confirm that the vegetation parameters in this dataset are representative.

Figures 5a and 5b show the soil water contents in the rooting zone and in the recharge layer for M1 and M2. The field observations also provide a measure of the water content in these two layers. The soil water in the rooting zone is close to that observed. However, the recharge layer is quite different: in the model, the third layer loses water persistently, while the observations

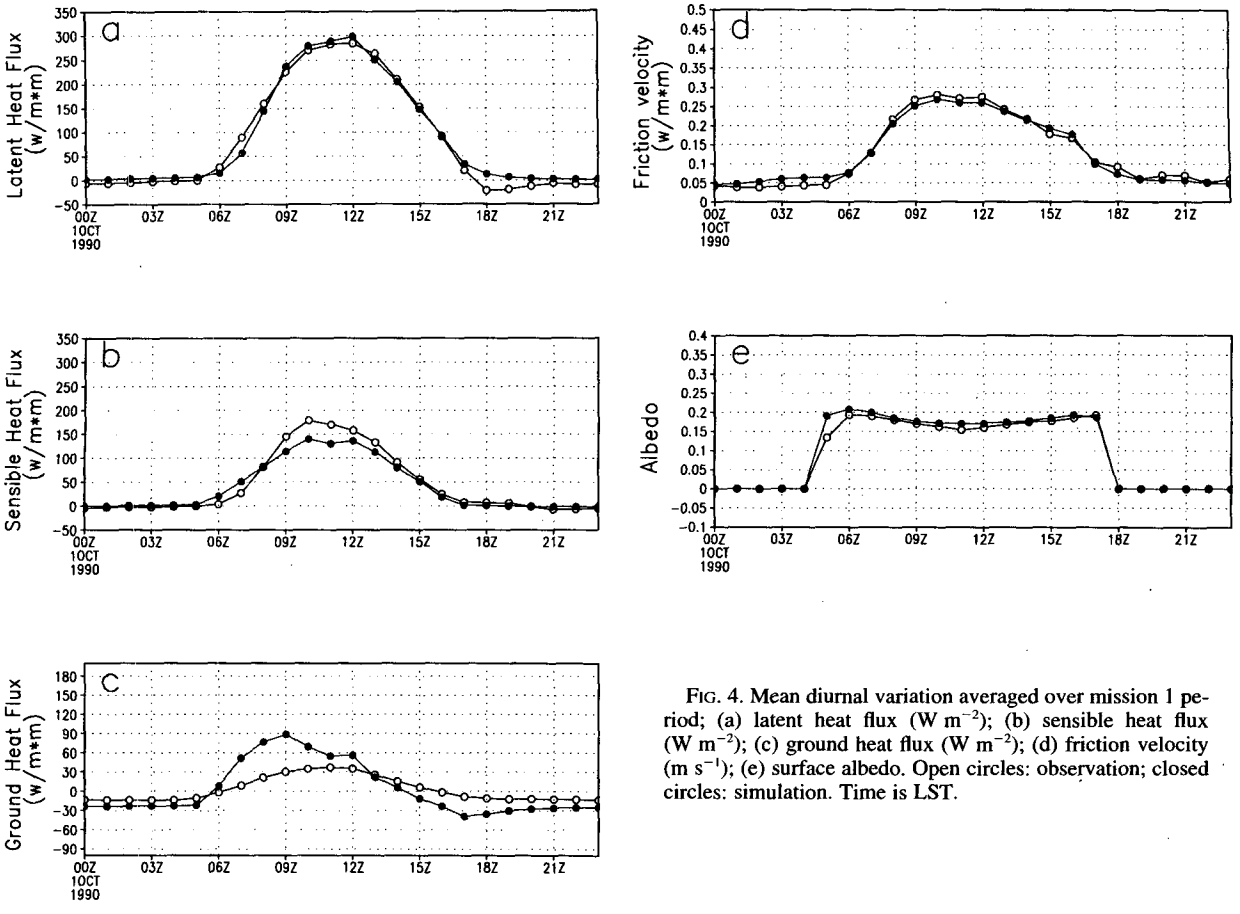

FIG. 4. Mean diurnal variation averaged over mission 1 period; (a) latent heat flux (W m^{-2}); (b) sensible heat flux (W m^{-2}); (c) ground heat flux (W m^{-2}); (d) friction velocity (m s^{-1}); (e) surface albedo. Open circles: observation; closed circles: simulation. Time is LST.

remain constant. To maintain the model's water balance, part of the water for evaporation has to come from the deeper soil layer. In particular, for M1 the total rainfall is only 13.4 mm. The total simulated evaporation for this period is 93.7 mm. Since the water content in the rooting zone has no substantial reduction, the third layer in the model must lose water. In the observations, it seems some water might come from other sources.

5. Sensitivity to the vegetation parameters

a. Off-line test

The validation results presented in the previous section show that SSiB is able to simulate the fluxes and radiation components well for the deforestated site using DATA N and observed atmospheric forcing. However, this new vegetation dataset is quite different from those used in previous deforestation studies. In a previous Amazon study (Nobre et al. 1991), degraded pasture was used to represent surface conditions in the deforestation scenario and characteristic parameter values for this vegetation type were drawn from the ecological literature. The main vegetation parameters in Nobre et al.'s deforestation studies are shown in Table 1 as DATA P. There are several substantial differences between DATA P and DATA N. The leaf area index is much higher in DATA P since it has a two story vegetation. The total leaf area index in DATA P is about 4, while in DATA N the leaf area indexes are 1, and 2 for M1 and M2, respectively. The soil properties between these two datasets are also quite different. DATA N has one order of magnitude higher soil conductivity at saturation, and about five times less soil water potential at saturation. The total soil depth for DATA P is larger than that for DATA N. The surface roughness length in DATA P is about three times higher than that of DATA N. In the Nobre et al. (1991) experiments, the mean surface albedo for the deforested cases was 0.25. Observational evidence has since shown that this number is unrealistically high (Bastable et al. 1993), mainly because the soil background reflectance is observed to be much lower in cleared area than was assumed in Nobre et al. (1991). In a later numerical experiment (Dirmeyer 1992), the albedo in deforestation experiments was reduced to about 0.18, which is very close to the value in DATA N.

Using DATA N as well as meteorological forcings from M1 and M2, off-line tests were conducted. Fig-

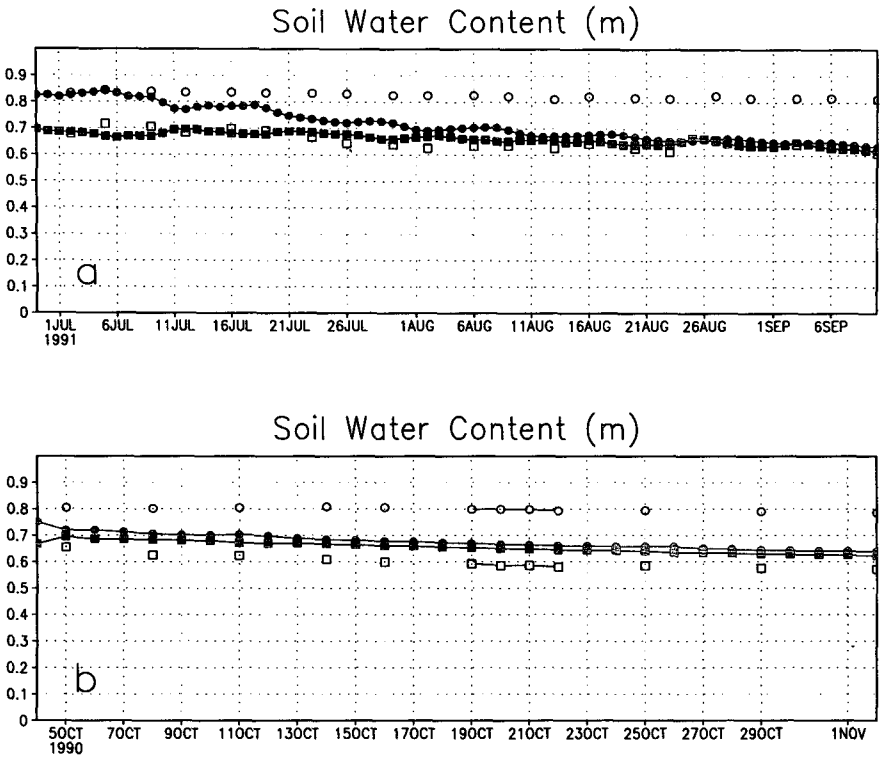

FIG. 5. Soil water content (m) at the recharge zone (observation: open circles; simulation: closed circles) and rooting layer (observation: open squares; simulation: closed squares). (a) Mission 2. (b) Mission 1.

ures 6a and 7a show the mean diurnal variation of latent heat fluxes for the M1 and M2 periods. The maximum simulated latent heat fluxes using DATA P are about 40 W m^{-2} more during M1 and about 10 W m^{-2} more during M2 than those in DATA N. Correspondingly, the simulated sensible heat fluxes are lower during M1. These differences persist throughout the integration period. Precipitation during M1 averages 0.44 mm day^{-1}, whereas the figure for M2 is 3.3 mm day^{-1}. The land surface conditions greatly affect evaporation during M1 (a dry period). The simulated friction velocity using DATA P is quite different from the observations (not shown), which shows that the vegetation structure in DATA P are significantly different from the vegetation at the ABRACOS experimental site.

To test the causes for such big differences between the results obtained using DATA N and DATA P, we examined the response of the off-line model to individual parameter changes. The forcing data from M1 and M2 were used to drive the off-line model in these experiments. Except for the sorption parameter B and hydraulic conductivity at saturation K_s, which are highly correlated, we changed one parameter at a time to test the model response to such change. Parameters K_s and B were determined based on the data of Clapp and Hornberger (1978), and have a similar impact on the evaporation rate. Another soil property parameter, the soil moisture at saturation (Ψ_s), has a different effect and was varied separately from K_s and B.

Table 3 shows the mean latent heat flux and average maximum latent heat flux from the experiments using DATA N and DATA P, and the sensitivity tests. Some parameters have virtually no impact on the evaporation and are not shown in the table. The mean values are averaged over the entire integration period.

Since the major differences in latent heat flux between DATA N and DATA P appear around noon (Figs. 6a and 7a), we list both the mean values and the mean maximum values in Table 3. The sum of the maximum latent heat flux (MLH) differences from individual parameter changes differ significantly from the differences between DATA N and DATA P; 73 W m^{-2} for M1 and 9 W m^{-2} for M2. The mean values from these two sets are close. Due to the nonlinear interaction, the sum of each individual effect in Table 3 is not equal to the difference by using the whole DATA N and DATA P. But individual parameter tests reveal the most important parameters and physical processes involved in the land surface–atmosphere interactions.

Among vegetation parameters in this study, the leaf area index (LAI) plays the most important role in increasing the evaporation. We tested the relationship be-

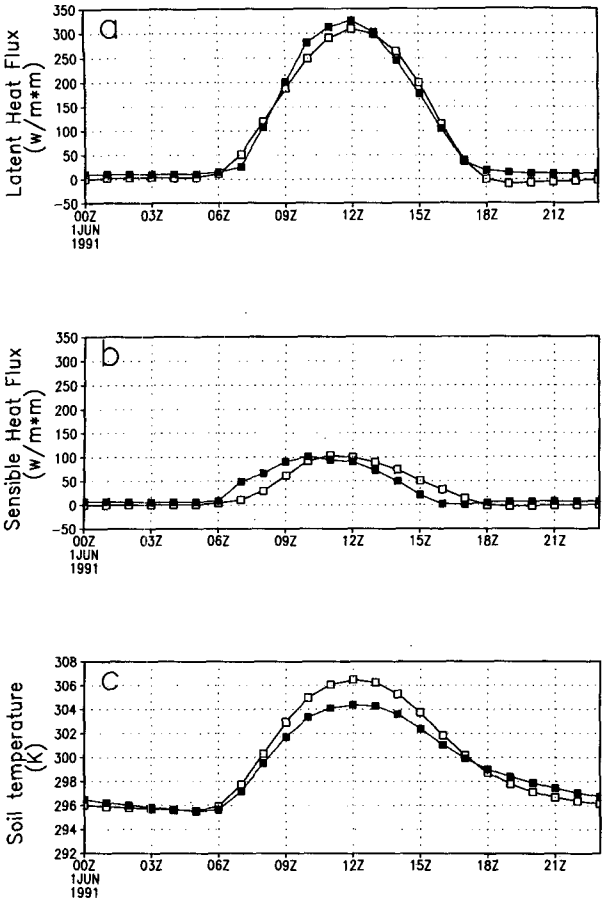

FIG. 6. Mean diurnal variation averaged over mission 2 period using DATA P; (a) latent heat flux (W m^{-2}); (b) sensible heat flux (W m^{-2}); open circles: observation; closed circles: simulation; (c) surface temperature (K); open circles: using DATA N; closed circles: using DATA P. Time is LST.

tween LAI and evaporation using forcing data from M1 and M2. The changes in latent heat flux with LAI are quite linear. When the LAI is reduced from 4 to 1, the MLH decreases by about 60 W m^{-2}. Higher LAIs are associated with lower canopy resistances. For LAIs larger than 5, the MLH almost reaches saturation in these experiments.

The impact of soil properties is also significant. Higher soil water potential at saturation helps the soil water reach the surface for evaporation. The difference in the MLH by using the new Ψ_s is about 60 W m^{-2}. Deeper soils hold more soil water for evaporation. Hydraulic conductivity is proportional to hydraulic conductivity at saturation, and inversely related to the sorption constant B. The low K_s and high B in DATA P tends to slow the diffusion process and thus reduces the evaporation rate. Table 3 shows that the reduction is significant, but is still not large enough to compensate for other parameters' impacts. The total evaporation rate is increased by using DATA P.

Large changes in the surface energy balance lead to changes in the surface temperature. Figures 6c and 7c show the diurnal variation in soil temperature using DATA N for M2 and M1, respectively. The simulated surface temperature using DATA N is systematically higher than DATA P. The average increase over the entire period is about 0.5 K.

b. Sensitivity using the GCM

The impacts of using parameters associated with DATA N and DATA P were tested in the Center for Ocean–Land–Atmosphere Studies General Circulation Model (COLA GCM). Although DATA P has been tested in the COLA GCM before (Nobre et al. 1990; Dirmeyer 1992; Dirmeyer and Shukla 1994) several improvements in the GCM have been made since those experiments were conducted. We decided to reintegrate the model using DATA P. The tests in this study were intended to evaluate the sensitivity of the

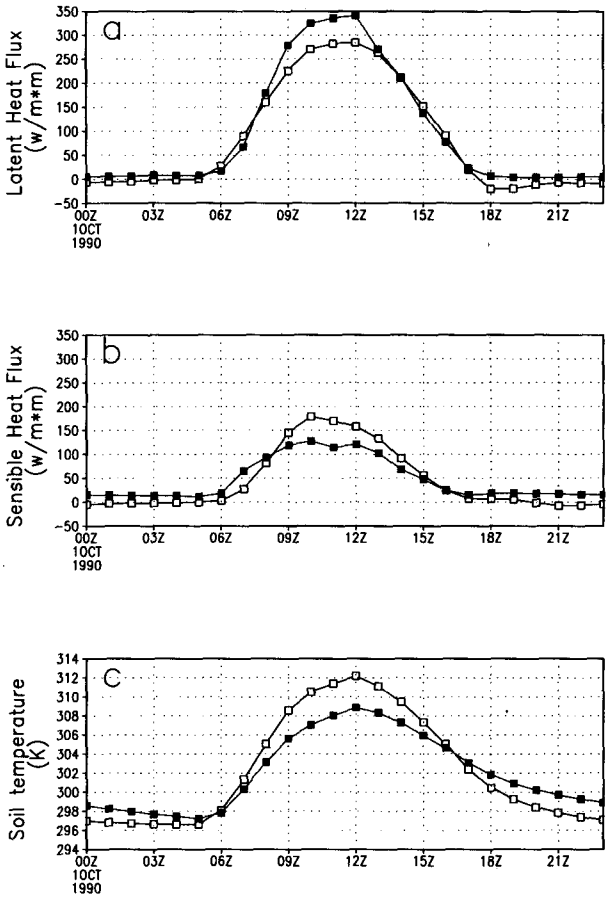

FIG. 7. Mean diurnal variation averaged over mission 1 period using DATA P; (a) latent heat flux (W m^{-2}); (b) sensible heat flux (W m^{-2}); open circles: observation; closed circles: simulation; (c) surface temperature (K); open circles: using DATA P; closed circles: using DATA P. Time is LST.

TABLE 3. Latent heat fluxes (W m^{-2}) from sensitivity tests.

		Mission 1				Mission 2			
		Maximum		Mean		Maximum		Mean	
			Dif		Dif		Dif		Dif
	DATA N	298		88		316		93	
	DATA P	341	43	97	9	326	10	95	2
1	LAI = 4	362	64	106	18	339	23	97	4
2	Soil depth 3.49 m	338	40	101	13	323	7	95	2
3	$\Psi_s = -0.153$	365	67	106	18	339	23	99	6
4	Adjustment factor for temperature (308, 276, 327)	321	23	93	5	330	14	96	3
5	$K_s = 0.2E - 5$, $B = 10.4$	195	−103	34	−44	282	−34	77	−16
6	Porosity 0.42	280	−18	80	−7	339	−24	99	−6
	Total difference (1–4)		194		54		67		15
	Total difference (5–6)		−121		−51		−58		−22

model to changes in the surface parameters and were not designed to predict the impact of Amazonian deforestation on climate.

The COLA GCM is based on a modified version of the National Centers for Environmental Prediction (formerly National Meteorological Center) global spectral model with rhomboidal truncation at zonal wavenumber 40 (Sela 1980; Kinter et al. 1988; Fennessy et al. 1994). The prognostic computations in COLA GCM are conducted in the spectral domain and the physical processes are computed on a grid (approximately 1.8° latitude by 2.8° longitude). The model is discretized into 18 vertical layers.

The parameterizations for physical processes include an efficient radiation scheme, which resolves the diurnal cycle and includes terrestrial radiative heating (Harshvardhan et al. 1987) and solar radiative heating (Lacis and Hansen 1974; modified by Davies 1982).

TABLE 4. Vegetation data and initial conditions in GCM simulations.

	Vegetation parameters	Initial conditions
Case 1N1	DATA N/M1	1 June 1991
Case 1N2	DATA N/M1	1 June 1992
Case 1N3	DATA N/M1	1 June 1993
Case 1P1	DATA P	1 June 1991
Case 1P2	DATA P	1 June 1992
Case 1P3	DATA P	1 June 1993
Case 1c1	Tropical rainforest	1 June 1991
Case 1c2	Tropical rainforest	1 June 1992
Case 1c3	Tropical rainforest	1 June 1993
Case 2N1	DATA N/M2	15 September 1990
Case 2N2	DATA N/M2	15 September 1991
Case 2N3	DATA N/M2	15 September 1992
Case 2P1	DATA P	15 September 1990
Case 2P2	DATA P	15 September 1991
Case 2P3	DATA P	15 September 1992
Case 2c1	Tropical rainforest	15 September 1990
Case 2c2	Tropical rainforest	15 September 1991
Case 2c3	Tropical rainforest	15 September 1992

An interactive cloud scheme, which is similar to the one developed by Slingo (1987), was incorporated into the GCM for the radiation calculations (Hou 1990). The COLA GCM also includes the level 2.0 second-order turbulence closure scheme of Mellor and Yamada

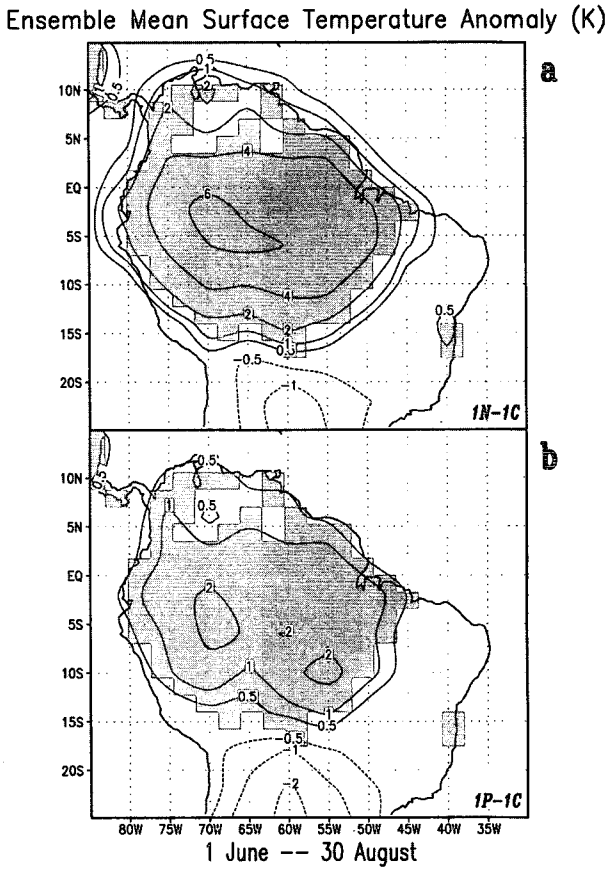

FIG. 8. Three-month mean difference in surface temperature for (a) ensemble 1N minus ensemble 1c; (b) ensemble 1P minus ensemble 1c. Units are kelvins.

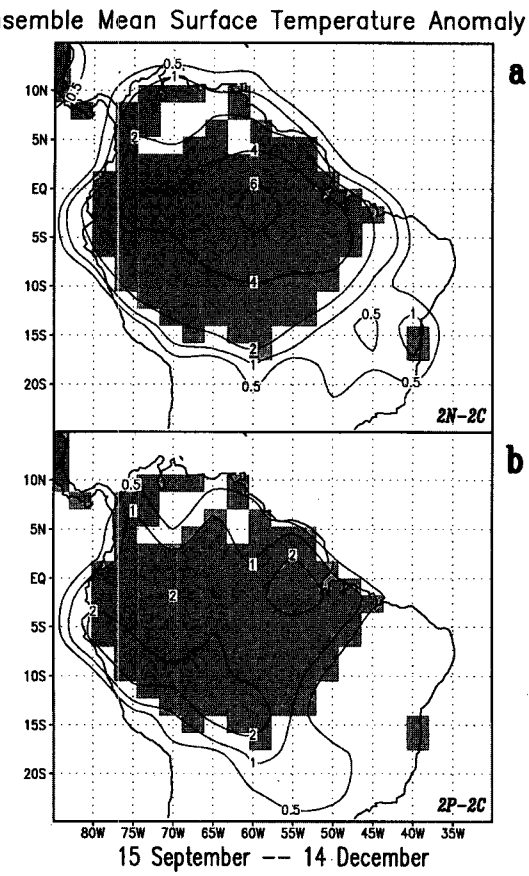

FIG. 9. Three-month mean difference in surface temperature for (a) ensemble 2N minus ensemble 2c; (b) ensemble 2P minus ensemble 2c. Units are kelvins.

(1982) for subgrid-scale exchanges of heat, momentum, and moisture; a modified Kuo scheme for convection (Anthes 1977; Kuo, 1965), shallow convection (Tiedke 1984), and large-scale condensation. SSiB is used to model the surface layer in the COLA GCM.

Using the ABRACOS vegetation data, several numerical experiments with different vegetation properties for deforestation were conducted. Due to the internal variability in the GCM, each scenario consists of three cases with initial conditions from different years. The results from three case ensembles are presented in this paper. The averages of cases 1N1, 1N2, and 1N3 are referred to as ensemble 1N. The averages of cases 1P1, 1P2, and 1P3 are referred to as ensemble 1P, etc. (See Table 4 for detailed information about each case).

In the two control ensembles (ensembles 1c and 2c), the Amazon Basin is completely covered by tropical rainforest. The vegetation parameters from M1 are used for ensemble 1N and the parameters from M2 are used for ensemble 2N. DATA P is used for ensembles 1P and 2P, but the albedo in these two experiments was also set to 0.18. The climatological sea surface temperature (SST) is used as the sea surface boundary conditions (Slutz et al. 1985). Ensembles 1 and 2 were integrated from 1 June to 30 August and 15 September to 14 December, respectively.

Figures 8a, 8b, 9a, and 9b show the surface temperature anomalies for ensembles 1N, 1P, 2N, and 2P, respectively. The shaded areas in the figures illustrate the extent of the deforestation area. Although both datasets produce positive temperature anomalies, the surface temperatures in ensembles 1N and 2N rise much higher, consistent with the off-line test. However, while the off-line test only showed a half-degree difference, the differences between ensembles 1N and 1P, and 2N and 2P are about 2–3 K. Positive cloud feedback appears to have amplified this impact. Meanwhile, the anomaly patterns also show some differences. The new data created more uniform temperature increases over the entire deforestation area. The positive anomalies using the previous data were maximum in the southwest part of the deforestation area.

The surface energy budget is shown in Table 5. The values in Table 5 are averaged over the shaded areas in Fig. 8, excluding central America and the area located at 15°S, 40°W. The downward shortwave radiation is increased in every deforestation case due to reduction in cloudiness. The new parameters lead to an increase in downward shortwave radiation because of the reduced evaporation relative to results produced by the previous parameters. The upward shortwave radi-

TABLE 5a. Surface and budget terms for ensemble 1*. The units for all variables except temperature are watts per square meter.

		Ensemble 1N		Ensemble 1P	
Variables	Ensemble 1c	Changes	Percent changes	Changes	Percent changes
Surface T (K)	298.4	+3.1		+1.4	
Latent	109	−25	−23%	−10	−9%
Sensible	54	+7	+14%	−5	−9%
Soil heat	5.3	−1.5	−28%	+0.1	+2%
SW down	232	+13	+5%	+9	+4%
SW up	31	+12	+37%	+11	+35%
LW down	418	−1	0	−4	−1%
LW up	450	+21	+5%	+9	+2%

TABLE 5b. Surface and budget terms for ensemble 2.

Variables	Ensemble 2c	Ensemble 2N		Ensemble 2P	
		Changes	Percent changes	Changes	Percent changes
Surface T (K)	296.4	+3.3		+1.0	
Latent	95	−37	−39%	−10	−11%
Sensible	43	+19	+44%	−2	−5%
Soil heat	6.7	−1.0	−13%	+0.5	+7%
SW down	218	+20	+9%	+9	+4%
SW up	30	+12	+39%	+10	+33%
LW down	395	−6	−1%	−5	−1%
LW up	439	+22	+5%	+7	+1%

ation is almost unchanged because the albedo in all the deforestation cases is similar. The downward longwave radiation has no substantial change in all cases. To maintain the energy balance, larger upward longwave radiation flux and higher temperatures in ensemble 1N and ensemble 2N are simulated.

The most significant differences occurred in the latent heat flux simulations (Figs. 10 and 11). There were only small evaporation rate changes in ensembles 1P and 2P; the average latent heat flux reduction over the entire deforestation area is only 10 W m^{-2}. Using DATA N, there were substantial reductions in evaporation rates in both ensemble 1N and ensemble 2N. The average reductions are about 25 W m^{-2} for ensemble 2N and 37 W m^{-2} for ensemble 1N, which are three times higher than these obtained using DATA P. The

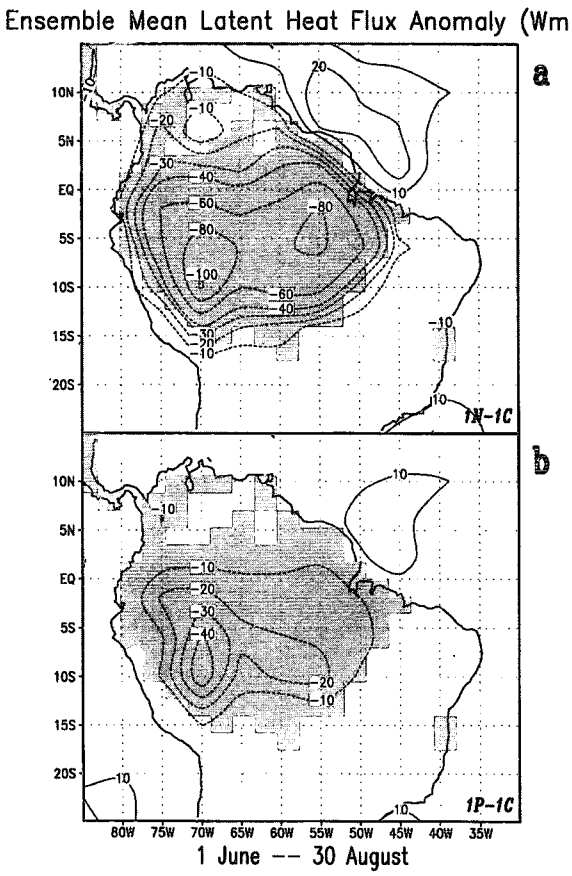

FIG. 10. Three-month mean difference in latent heat flux for (a) ensemble 1N minus ensemble 1c; (b) ensemble 1P minus ensemble 1c. Units are watts per square meter.

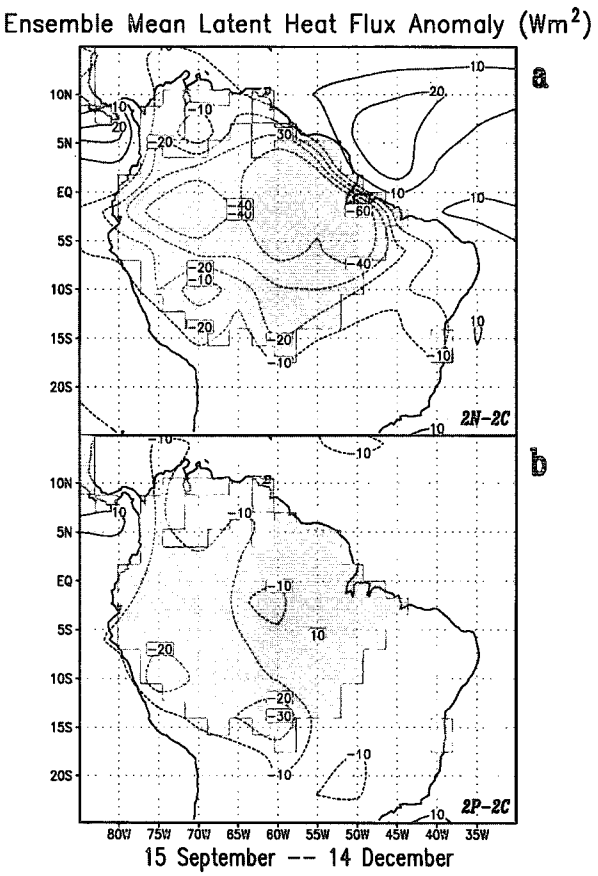

FIG. 11. Three-month mean difference in latent heat flux for (a) ensemble 2N minus ensemble 2c; (b) ensemble 2P minus ensemble 2c. Units are watts per square meter.

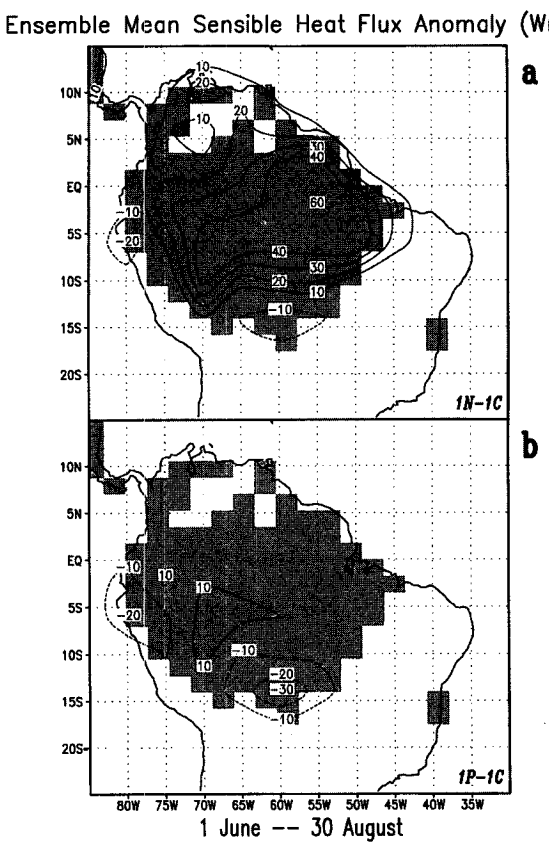

FIG. 12. Three-month mean difference in sensible heat flux for (a) ensemble 1N minus ensemble 1c; (b) ensemble 1P minus ensemble 1c. Units are watts per square meter.

differences obtained by using different datasets are again amplified by the interaction processes.

The main flux changes observed when using DATA P are manifested in the reduction of sensible heat flux (Figs. 12 and 13). Although the mean over the entire deforestated area shows no major difference, the reduction in some areas is quite significant. In ensembles 1N and 2N, the changes in the sensible heat fluxes are in the opposite direction to the latent heat flux changes; they increased by 10–20 W m^{-2} over the cleared area. These changes were consistent with those associated with other land surface change sensitivity studies (Xue and Shukla 1993; Xue et al. 1995; Xue 1995, personal communication).

The differences in the simulated surface fluxes and temperatures produced by using different vegetation datasets are significant. Such differences would certainly cause a response in the atmosphere. The preliminary results from this study show that the precipitation and moisture flux convergence are quite different when using DATA N versus DATA P. In this paper, we have limited our investigation to the surface energy balance; we will not further examine atmospheric effects here.

6. Summary

SSiB has been recalibrated and tested using the ABRACOS dataset. The results show that this model is capable of realistically simulating the latent heat flux, sensible heat flux, and momentum flux by using observed vegetation parameters. The differences between simulated and observed latent heat and sensible heat fluxes are less than 10 W m^{-2}. The differences between observed and simulated latent heat fluxes occurred mainly at night. The observations show that dew was often produced at night, whereas the model failed to simulate this phenomena. There is a temporal phase problem in the ground heat flux simulation; this is largely due to the force–restore method used in SSiB. Nonetheless, the simulated daily mean of the ground heat flux was close to the observations.

The new vegetation dataset from ABRACOS has been compared with the data previously used for deforestation scenarios. Compared to previous deforestation experiments, the new vegetation dataset produced significantly different latent heat fluxes and surface temperatures in off-line and GCM simulations. Using the new dataset to simulate widespread defor-

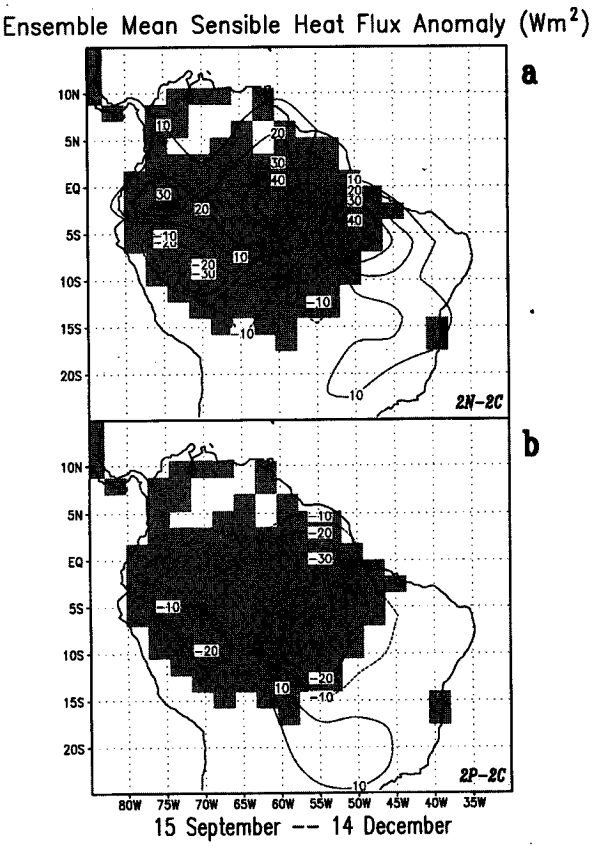

FIG. 13. Three-month mean difference in sensible heat flux for (a) ensemble 2N minus ensemble 2c; (b) ensemble 2P minus ensemble 2c. Units are watts per square meter.

estation of the Amazon in a GCM, simulated surface temperature was about 2 K higher and the simulated latent heat flux was about 25 W m^{-2} lower than that generated by a previous dataset. These differences can be expected to result in substantially different responses in rainfall and atmosphere circulation. Changes in some key parameters, particularly leaf area index and soil properties, seem to be particularly important.

During the last decade, much attention has been given to the impact of albedo and surface roughness. This study along with that of Xue et al. (1995) shows that besides the surface albedo, other vegetation and/or soil parameters may also play a major role in the land surface–atmosphere interactions. Most Amazon deforestation studies thus far were sensitivity studies per se. The deforestation data used in previous studies have helped understanding the impact of land surface changes on the land surface–atmosphere interactions and climate. This study indicates a realistic description of the land surface condition is critical to a realistic assessment of the impact of land use change on climate.

Acknowledgments. The authors would like to thank Drs. J. Shukla, W. J. Shuttleworth, and C. Nobre for supporting this project. The data used in this study was from the ABRACOS project. Special thanks go to I. R. Wright for his help with the meteorological data, to M. G. Hodnett for assistance with the soil data, to Dr. A.-L. McWilliam for the vegetation parameters, and to D. Anderson for arranging additional computational support. Drs. J. Gash and the staff at the Institute of Hydrology (UK) and their Brazilian collaborators are thanked for the work done to compile the ABRACOS datasets. This work was conducted under support from the National Science Foundation (NSF) through NSF Grants ATM-93-41271, ATM-93-21354, and EAR-94-05431, and the National Oceanic and Atmospheric Administration (NOAA) through NOAA Grant NA46GP0340-02. Computational support was provided by the National Center for Atmospheric Research (NCAR) Scientific Computing Division and CRAY Research Inc.

REFERENCES

Anthes, R. A., 1977: A cumulus parameterization scheme utilizing a one-dimensional cloud model. *Mon. Wea. Rev.*, **105,** 270–300.

Bastable, H. G., W. J. Shuttleworth, R. L. G. Dallarosa, G. Fisch, and C. A. Nobre, 1993: Observations of climate, albedo and surface radiation over cleared and undisturbed Amazonian forest. *Int. J. Climatol.*, **13,** 783–798.

Businger, J. A., J. C. Wyngaard, Y. I. Zumi, and E. G. Bradley, 1971: Flux-profile relationships in the atmosphere surface layer. *J. Atmos. Sci.*, **28,** 181–189.

Camillo, P. J., and R. J. Gurney, 1986: A resistance parameter for bare-soil evaporation models. *Soil Sci.*, **2,** 95–105.

Clapp, R. B., and G. M. Hornberger, 1978: Empirical equations for some soil hydraulic properties. *Water Resour. Res.*, **14,** 601–604.

Davies, R., 1982: Documentation of the solar radiation parameterization in the GLAS Climate Model. NASA Tech. Memo 83961, 57 pp.

Dickinson, R. E., 1983: Land surface processes and climate surface albedos and energy balance. *Advances in Geophysics,* Vol. **25,** Academic Press, 305–353.

——, and A. Henderson-Sellers, 1988: Modelling tropical deforestation: A study of GCM land-surface parameterizations. *Quart. J. Roy. Meteor. Soc.*, **114,** 439–462.

Dirmeyer, P. A., 1992: GCM studies of the influence of vegetation on the general circulation: The role of albedo in modulating climate change. Ph.D. dissertation, University of Maryland College Park, 227 pp.

——, and J. Shukla, 1994: Albedo as a modulator of climate response to tropical deforestation. *J. Geophys. Res.*, **99,** 20 863–20 877.

Fennessy, M. J., J. L. Kinter III, B. Kirtman, L. Marx, S. Nigam, E. Schneider, J. Shukla, D. Straus, A. Vernerkar, Y. Xue, and J. Zhou, 1994: The simulation Indian monsoon: A GCM sensitivity study. *J. Climate,* **7,** 33–43.

Harshvardhan, R. Davies, D. A. Randall, and T. G. Corsetti, 1987: A fast radiation parameterization for general circulation models. *J. Geophys. Res.*, **92,** 1009–1016.

Henderson-Sellers, A., and V. Gornits, 1984: Possible climate impacts of land cover transformations with particular emphasis on tropical deforestation. *Climate Change,* **6,** 231–258.

——, R. E. Dickinson, T. B. Durbridge, P. J. Kennedy, K. McGuffie, and A. J. Pitman, 1993: Tropical deforestation: Modeling local to regional scale climate change. *J. Geophys. Res.* **98,** 7289–7316.

Hou, Y.-T., 1990: Cloud-radiation-dynamics interaction. Ph.D. dissertation, University of Maryland, 209 pp.

Jarvis, P. G., 1976: The interpretation of the variations in leaf water potential and stomatal conductance found in canopies in the field. *Philos. Trans. Roy. Soc. London, Ser. B.*, **273,** 593–610.

Kinter, J. L., III, J. Shukla, L. Marx, and E. K. Schneider, 1988: A simulation of the winter and summer circulations with the NMC global spectral model. *J. Atmos. Sci.*, **45,** 2486–2522.

Kuo, H. L., 1965: On formation and intensification of tropical cyclones through latent heat release by cumulus convection. *J. Atmos. Sci.*, **22,** 40–63.

Lacis, A. A., and J. E. Hanson, 1974: A parameterization for the absorption of solar radiation in the earth's atmosphere. *J. Atmos. Sci.*, **32,** 118–133.

Lean, J., and D. A. Warrilow, 1989: Simulation of the regional climatic impact of Amazonian deforestation. *Nature,* **342,** 411–413.

Lloyd, C. R., J. H. C. Gash, W. J. Shuttleworth, and A. de O. Marques Filho, 1988: The measurement and modelling of rainfall interception loss for Amazonian rain forest. *Agric. For. Meteor.*, **42,** 63–73.

Louis, J.-F., 1979: A parametric model of vertical eddy fluxes in the atmosphere. *Bound.-Layer Meteorol.*, **17,** 187–202.

McWilliam, A. L. C., J. M. Roberts, O. M. R. Cabral, M. V. B. R. Leitao, A. C. L. de Costa, G. T. Maitelli, and C. A. G. P. Zamporoni, 1993: Leaf area index and above ground biomass of terra firme rain forest and adjacent clearings in Amazonia. *J. Funct. Ecol.,*

Mellor, G. L., and T. Yamada, 1982: Development of a turbulence closure model for geophysical fluid problems. *Rev. Geophys. Space Phys.*, **20,** 851–875.

Nobre, C. A., P. J. Sellers, and J. Shukla, 1991: Amazonian deforestation and regional climate change. *J. Climate,* **4,** 957–988.

Paulson, C. A., 1970: Mathematical representation of wind speed and temperature profiles in the unstable atmospheric surface layer. *J. Appl. Meteor.*, **9,** 857–861.

Polcher, J., and K. Laval, 1994: The impact of African and Amazonian deforestation on tropical climate. *J. Hydrol.*, **155,** 389–405.

Sela, J. G., 1980: Spectral modelling at the National Meteorological Center. *Mon. Wea. Rev.*, **108,** 1279–1292.

Sellers, P. J., 1985: Canopy reflectance, photosynthesis and transpiration. *Int. J. Remote Sens.*, **6,** 1335–1372.

——, Y. Mintz, Y. C. Sud, and A. Dalcher, 1986: A simple biosphere model (SiB) for use within general circulation models. *J. Atmos. Sci.*, **43,** 505–531.

——, W. J. Shuttleworth, J. L. Dorman, A. Dalcher, and J. M. Roberts, 1989: Calibrating the simple biosphere model for Amazonian tropical forest using field and remote sensing data. Part I: Average calibration with field data. *J. Appl. Meteor.,* **28,** 727–759.

——, M. D. Heiser, and F. G. Gall, 1992: Relations between surface conductance and spectral vegetation indices as intermediate (100 m^2 to 15 km^2) length scale. *J. Geophys. Res.,* **97,** 19 033–19 060.

Shao, Y., and A. Henderson-Sellers, 1995: Soil moisture simulation workshop review. *Global and Plantery Change,* in press.

——, R. D. Anne, A. Henderson-Sellers, P. Irannejad, P. Thorton, X. Liang, T. H. Chen, C. Ciret, C. Desborough, O. Balachova, A. Haxeltine, and A. Ducharne, 1994: Soil Moisture simulation: A report of the RICE and PILPS workshop. *IGPO Publication Series,* No. 14, 179 pp.

Shukla, J., C. A. Nobre, and P. J. Sellers, 1990: Amazonian deforestation and climate change. *Science,* **247,** 1322–1325.

Shuttleworth, W. J., 1988: Evaporation from Amazonian rain forest. *Philos. Trans. Roy. Soc. London, Ser. B,* 233–346.

——, and Coauthors, 1984: Eddy correlation measurements of energy partition for Amazonian forest. *Quart. J. Roy. Meteor. Soc.,* **110,** 1143–1162.

——, J. H. C. Gash, C. R. Lloyd, C. J. Moore, J. M. Roberts, A. De O. Marques, G. Fisch, V. De P. Silva, M. N. G. Ribeiro, L. C. B. Molion, L. D. De Abrea Sa, C. A. Nobre, O. M. R. Cabral, S. R. Patel, and J. C. De Moraes, 1985: Daily variations of temperature and humidity within and above Amazonian forest. *Weather,* **40,** 102–108.

——, ——, J. M. Roberts, C. A. Nobre, L. C. B. Molion, and M. N. G. Ribeiro, 1991: Post-deforestation Amazonian climate: Anglo–Brazilian research to improve prediction. *J. Hydrol.,* **129,** 71–86.

Slingo, J. M., 1987: The development and verification of a cloud prediction scheme for the ECMWF model. *Quart. J. Roy. Meteor. Soc.,* **103,** 29–43.

Slutz, R. J., S. J. Lubker, J. D. Hiscox, S. D. Woodruff, R. L. Jenne, D. H. Joseph, P. M. Streuer, and J. D. Elms, 1985: COADS: Comprehensive Ocean–Atmosphere Data Set. Release 1, 262 pp. [Available from Climate Research Program, Environmental Research Laboratories, 325 Broadway, Boulder, CO 80303.]

Sud, Y. C., and W. E. Smith, 1984: Ensemble formulation of surface fluxes and improvement in evapotranspiration and cloud parameterization in a GCM. *Bound.-Layer Meteor.,* **29,** 185–210.

——, G. K. Walker, J.-H. Kim, G. E. Liston, and P. J. Sellers, 1995: Biogeophysical consequences of a tropical deforestation scenario: A GCM simulation study. *J. Climate,* in press.

Tiedtke, M., 1984: The effect of penetrative cumulus convection on the large-scale flow in a general circulation model. *Beitr. Phys. Atmos.,* **57,** 216–239.

Wright, I. R., J. H. C. Gash, H. R. Rocha, W. J. Shuttleworth, C. A. Nobre, P. R. A. Carvalho, M. V. B. R. Leitao, G. T. Maitelli, and C. A. G. P. Zamparoni, 1992: Dry season micrometeorology of Amazonian ranchland. *Quart. J. Roy. Meteor. Soc.,* **118,** 1083–1099.

Xue, Y., and J. Shukla, 1993: The influence of land surface properties on Sahel climate. Part I: Desertification. *J. Climate,* **6,** 2232–2245.

——, P. J. Sellers, J. L. Kinter III, and J. Shukla, 1991: A simplified biosphere model for global climate studies. *J. Climate,* **4,** 345–364.

——, M. J. Fennessy, and P. J. Sellers, 1995: Impact of vegetation properties on U.S. summer weather prediction. *J. Geophys. Res.,* in press.